Oriented Mesoporous Silica Films Obtained by Electro-Assisted Self-Assembly (EASA)

Aurélie Goux,[†] Mathieu Etienne,[†] Emmanuel Aubert,[‡] Claude Lecomte,[‡] Jaafar Ghanbaja,[§] and Alain Walcarius*

Laboratoire de Chimie Physique et Microbiologie pour l'Environnement, UMR 7564, CNRS-Institut Jean Barriol, Nancy-Université, 405, rue de Vandoeuvre, 54600 Villers-lès-Nancy, France, Laboratoire de Cristallographie, Résonance Magnétique et Modélisation, UMR 7036, CNRS-Institut Jean Barriol, Nancy-Université, BP 70239, Boulevard des Aiguillettes, 54506 Vandoeuvre-lès-Nancy Cedex, France, and Service commun de microscopies électroniques et microanalyses X, Faculté des Sciences, Nancy-Université, BP 70239, Boulevard des Aiguillettes, 54506 Vandoeuvre-lès-Nancy Cedex, France

Received October 31, 2008. Revised Manuscript Received December 17, 2008

Highly ordered and vertically oriented mesoporous silica films can be generated by electro-assisted self-assembly (EASA). The method involves the electrogeneration of hydroxide ions at an electrode surface immersed in an hydrolyzed sol solution (containing typically tetraethoxysilane, TEOS, and cetyltrimethylammonium bromide, CTAB) in order to catalyze polycondensation of the precursors and self-assembly of hexagonally packed one-dimensional channels that grow perpendicularly to the support. Vertically aligned mesostructures have been demonstrated by TEM imaging and by grazing incidence X-ray diffraction (GIXD), this latter technique enabling characterization of thin films directly on their underlying electrode surface. The influence of the electrosynthesis medium composition (precursor and surfactant concentrations, surfactant chain length) on the mesostructural order and film thickness has been thoroughly examined. It was shown that the highly ordered and oriented mesoporous silica films can be obtained over a wide composition of the starting sol (i.e., 10−200 mM CTAB and 50−350 mM TEOS) and that the lattice parameter can be moderately tuned by changing the chain length of the surfactant template. Thickness of these films can be accurately controlled by applying galvanostatic conditions and by varying the deposition time, which offer the versatility to be applied in the same way to electrodes of different nature without overpotential problems encountered in the potentiostatic mode. Thin mesoporous films are often covered with an additional byproduct made of particulate aggregates arising from bulk gelification at the electrode/solution interface. Getting aggregate-free thin films is possible by working in diluted solutions (i.e., [TEOS] < 125 mM and CTAB/TEOS ratio <0.32) and with a short deposition time (∼10 s). Voltammetric experiments carried out on these films deposited onto planar indium−tin-oxide electrodes, after template extraction, have revealed very sensitive responses to solution-phase redox probes as a result of fast mass transport from the external solution through the film to the electrode surface. Quantitative characterization of these mass transfer processes reveals that apparent diffusion coefficients as high as about 1×10^{-7} cm^2 s^{-1} can be reached but great care should be taken in defining the film synthesis conditions that may lead to some additional limiting effects.

1. Introduction

Ordered mesoporous silica-based materials discovered through innovative combinations of micellar and lyotropic liquid-crystal phases with sol−gel processing of silicate precursors[1] offer a great versatility to control the structure, texture, and functionality for advanced applications in various fields.[2] Indeed, soft matter organization at the mesoscale is likely to provide attractive templates to design a wide range of highly ordered mesoporous materials,[3] which can be functionalized via either postsynthesis grafting or in one step by self-assembly co-condensation to generate mesoporous organic−inorganic hybrid materials.[4] The majority of these

* Corresponding author. Tel: 33 (0)3 83 68 52 59. Fax: 33 (0)3 83 27 54 44. E-mail: alain.walcarius@lcpme.cnrs-nancy.fr.

[†] UMR 7564, CNRS-Institut Jean Barriol, Nancy-Université.

[‡] UMR 7036, CNRS-Institut Jean Barriol, Nancy-Université.

[§] Faculté des Sciences, Nancy-Universite.

(1) (a) Kresge, C. T.; Leonowicz, M. E.; Roth, W. J.; Vartuli, J. C.; Beck, J. S. *Nature* **1992**, *359*, 710. (b) Beck, J. S.; Vartuli, J. C.; Roth, W. J.; Leonowicz, M. E.; Kresge, C. T.; Schmitt, K. D.; Chu, C.T.-W.; Olson, D. H.; Sheppard, E. W.; McCullen, S. B.; Higgins, J. B.; Schlenker, J. L. *J. Am. Chem. Soc.* **1992**, *114*, 10834.

(2) (a) Stein, A.; Melde, B. J.; Schröden, R. C. *Adv. Mater.* **2000**, *12*, 1403. (b) Sanchez, C.; Julian, B.; Belleville, P.; Popall, M. *J. Mater. Chem.* **2005**, *15*, 3559. (c) Hartmann, M. *Chem. Mater.* **2005**, *17*, 4577. (d) Walcarius, A. *C. R. Chim.* **2005**, *8*, 693. (e) Clark, J. H.; MacQuarrie, D. J.; Tavener, S. J. *Dalton Trans.* **2006**, 4297. (f) Slowing, I. I.; Trewyn, B. G.; Giri, S.; Lin, V. S.-Y. *Adv. Funct. Mater.* **2007**, *17*, 1225.

(3) (a) de Soler-Illia, G. J.; Sanchez, C.; Lebeau, B.; Patarin, J. *Chem. Rev.* **2002**, *102*, 4093. (b) Lin, H.-P.; Mou, C.-Y. *Acc. Chem. Res.* **2002**, *35*, 927. (c) Berggren, A.; Palmqvist, A. E. C.; Holmberg, K. *Soft Matter* **2005**, *1*, 219. (d) Wan, Y.; Zhao, D. *Chem. Rev.* **2007**, *107*, 2821.

(4) (a) Sanchez, C.; Soler-Illia, G.J.D.A.A.; Ribot, F.; Grosso, D. *C. R. Chim.* **2003**, *6*, 1131. (b) Kickelbick, G. *Angew. Chem., Int. Ed.* **2004**, *43*, 3102. (c) Lebeau, B.; Patarin, J.; Sanchez, C. *Adv. Technol. Mater. Mater. Process. J.* **2004**, *6*, 298. (d) Vinu, A.; Hossain, K. Z.; Ariga, K. *J. Nanosci. Nanotechnol.* **2005**, *5*, 347. (e) Hoffmann, F.; Cornelius, M.; Morell, J.; Froeba, M. *Angew. Chem., Int. Ed.* **2006**, *45*, 3216. (f) Wan, Y.; Zhang, D.; Hao, N.; Zhao, D *Int. J. Nanotechnol.* **2007**, *4*, 66. (g) Antonietti, M.; Niederberger, M.; Smarsly, B. *Dalton Trans.* **2008**, 18.

10.1021/cm8029664 CCC: $40.75
Published on Web 01/29/2009

solids are prepared in the form of powders or monoliths; however, major advances have been achieved recently in the field of periodically organized mesoporous silica thin films because this shape is expected to facilitate materials integration in devices (including the miniaturized ones) for target applications (e.g., electrochemical and optical sensors, low-*k* materials in microelectronics, photovoltaic cells and photonic devices, membranes and separation techniques, or biomaterials).[5] Design, synthesis, and properties of mesoporous thin films (silica- and non-silica-based materials including organic−inorganic hybrids) have been extensively reviewed and nicely discussed in a recent, excellent, and comprehensive paper by the Sanchez group.[6]

Pioneering works on mesoporous silica thin films dated from the mid 1990s.[7] They were mostly based on chemical solution deposition methods in which mesostructuration occurs through evaporation-induced self-assembly (EISA) from a hydro-alcoholic sol solution.[8] Afterward, comprehensive control of the various parameters affecting the EISA mechanism (solvent evaporation, film water content equilibration with the atmosphere, spatial arrangement of template/inorganic interfaces, consolidation of the inorganic network) has been achieved. This has led to possible fine-tuning of the mesostructure types (2D-hexagonal, lamellar, wormlike, or tridimensional), of the pore size and thickness of silica walls (including materials with multimodal porosity), and of the film thickness (typically from 50 nm to 2 μm).[6] Today, EISA remains the most commonly used approach to generate mesoporous silica thin films even if some other methods (impregnation of copolymer layers,[9] self-standing film growing at liquid/liquid or liquid/air interfaces,[10] or pulsed laser deposition[11]) have also been reported. Functionalized hybrid mesoporous thin films can be also obtained through EISA, mostly by self-assembly co-condensation of a mixture of alkoxysilane and organoalkoysilane (or silsesquioxane) precursors in the presence of a surfactant template, giving rise to mesostructured deposits bearing a wide range of organofunctional groups.[6,12,13] Note that the functionalization level was usually restricted to organic/silica molar ratio up to 20% in order to keep a good level of mesostructural order. The postsynthesis grafting route, though largely exploited to derivatize mesoporous silica powders,[4] was less applied to the functionalization of thin films.[6]

In recent years, many efforts have been devoted to promote directed assembly of mesophases because tunable orientation of the mesoporous network is highly required for numerous applications. In particular, orientation of the porous framework orthogonal to the underlying substrate can be of great interest (e.g., to promote effective mass transport) but this is not so simple,[14] as most oriented 2D-hexagonal mesostructures prepared by EISA were characterized by mesopore channels parallel to the substrate.[7i,15] Among the strategies reported to generate mesoporous silica films with perpendicular or quasi orthogonal mesochannels, one can cite (1) sol−gel silica deposition through cylindrical domains of preassembled block copolymer films[16] or (2) through exotemplate membranes (i.e., dimensional confinement of the self-assembly process[17]); (3) the resort to patterned supports or combination of photoaligning and micropatterning techniques;[18] (4) epitaxial growth;[19] (5) magnetically induced orientation[20] (even if this approach was mainly applied to get highly ordered mesochannels oriented parallel to the support[21]). As most these fabrication methods were based on block polymers, the pore size of mesopore channels was usually larger than 5 nm or even much more.[16]

(5) (a) Ogawa, M. *Curr. Top. Colloid Interface Sci.* **2001**, *4*, 209. (b) Chao, K.; Liu, P.; Huang, K. C. R. *Chim.* **2005**, *8*, 727. (c) Nicole, L.; Boissiere, C.; Grosso, D.; Quach, A.; Sanchez, C. *J. Mater. Chem.* **2005**, *15*, 3598. (d) Innocenzi, P.; Kidchob, T.; Falcaro, P.; Takahashi, M. *Chem. Mater.* **2008**, *20*, 607. (e) Walcarius, A.; Kuhn, A. *Trends Anal. Chem.* **2008**, *27*, 593.

(6) Sanchez, C.; Boissiere, C.; Grosso, D.; Laberty, C.; Nicole, L. *Chem. Mater.* **2008**, *20*, 682.

(7) (a) Ogawa, M. *J. Am. Chem. Soc.* **1994**, *116*, 7941. (b) Ogawa, M. *Chem. Commun.* **1996**, 1149. (c) Anderson, M. T.; Martin, J. E.; Odinek, J.; Newcomer, P. In *Microporous & Macroporous Materials*; Lobo, R. F., Beck, J. S., Suib, S. L., Corbin, D. R., Davi, M. E., Iton, L. E., Zones, S. I., Eds.; Materials Research Society: Pittsburgh, PA, 1996; Vol. 431, p 217. (d) Yang, H.; Coombs, N.; Sokolov, I.; Ozin, G. A. *Nature* **1996**, *381*, 589. (e) Yang, H.; Coombs, N.; Sokolov, I.; Ozin, G. A. *J. Mater. Chem.* **1997**, *7*, 1285. (f) Yang, H.; Coombs, N.; Dag, O.; Sokolov, I.; Ozin, G. A. *J. Mater. Chem.* **1997**, *7*, 1755. (g) Lu, Y.; Ganguli, R.; Drewien, C. A.; Anderson, M. T.; Brinker, C. J.; Gong, W.; Guo, Y.; Soyez, H.; Dunn, B.; Huang, M. H.; Zink, J. I. *Nature* **1997**, *389*, 364. (h) Brinker, C. J. *Curr. Opin. Colloid Interface Sci.* **1998**, *3*, 166. (i) Yang, H.; Coombs, N.; Ozin, G. A. *J. Mater. Chem.* **1998**, *8*, 1205. (j) Ogawa, M.; Kikuchi, T. *Adv. Mater.* **1998**, *10*, 1077.

(8) (a) Brinker, C. J.; Lu, Y.; Sellinger, A.; Fan, H. *Adv. Mater.* **1999**, *11*, 579. (b) Grosso, D.; Cagnol, F.; Soler-Illia, G.J.D.A.A.; Crepaldi, E. L.; Amenitsch, H.; Brunet-Bruneau, A.; Bourgeois, A.; Sanchez, C. *Adv. Funct. Mater.* **2004**, *14*, 309. (c) Soler-Illia, G. J. A. A.; Innocenzi, P. *Chem.−Eur. J.* **2006**, *12*, 4478.

(9) (a) Nishiyama, N.; Tanaka, S.; Egashira, Y.; Oku, Y.; Ueyama, K. *Chem. Mater.* **2003**, *15*, 1006. (b) Tanaka, S.; Nishiyama, N.; Oku, Y.; Egashira, Y.; Ueyama, K. *J. Am. Chem. Soc.* **2004**, *126*, 4854.

(10) (a) Faget, L.; Berman, A.; Regev, O. *Thin Solid Films* **2001**, *386*, 6. (b) Liu, C.; Wang, J.; Li, B. *J. Non-Cryst. Solids* **2005**, *351*, 409.

(11) Balkus, K. J.; Scott, A. S.; Gimon-Kinsel, M. E.; Blanco, J. H. *Microporous Mesoporous Mater.* **2000**, *38*, 97.

(12) (a) Brinker, C. J. *MRS Bull.* **2004**, *29*, 631. (b) Fan, H.; Brinker, C. J. *Stud. Surf. Sci. Catal.* **2004**, *148*, 213.

(13) (a) Fan, H.; Reed, S.; Baer, T.; Schunk, R.; Lopez, G. P.; Brinker, C. J. *Microporous Mesoporous Mater.* **2001**, *625*, 44–45. (b) Etienne, M.; Walcarius, A. *Electrochem. Commun.* **2005**, *7*, 1449. (c) Zhang, X.; Wu, W.; Wang, J.; Liu, C. *J. Am. Ceram. Soc.* **2007**, *90*, 965. (d) Wahab, M. A.; Sudhakar, S.; Yeo, E.; Sellinger, A. *Chem. Mater.* **2008**, *20*, 1855.

(14) Brinker, C. J.; Dunphy, D. R. *Curr. Opin. Colloid Interface Sci.* **2006**, *11*, 126.

(15) Song, C.; Villemure, G. *Microporous Mesoporous Mater.* **2001**, *679*, 44–45.

(16) (a) Koganti, V. R.; Rankin, S. E. *J. Phys. Chem. B* **2005**, *109*, 3279. (b) Freer, E. M.; Krupp, L. E.; Hinsberg, W. D.; Rice, P. M.; Hedrick, J. L.; Cha, J. N.; Miller, R. D.; Kim, H.-C. *Nano Lett.* **2005**, *5*, 2014. (c) Eggiman, B. W.; Tate, M. P.; Hillhouse, H. W. *Chem. Mater.* **2006**, *18*, 723. (d) Dutreilh-Colas, M.; Yan, M.; Labrotr, P.; Delorme, N.; Gibaud, A.; Bardeau, J.-F. *Surf. Sci.* **2008**, *602*, 829. (e) Nagarajan, S.; Li, M.; Pai, R. A.; Bosworth, J. K.; Busch, P.; Smilgies, D.-M.; Ober, C. K.; Russel, T. P.; Watkins, J. J. *Adv. Mater.* **2008**, *20*, 246.

(17) (a) Yamaguchi, A.; Uejo, F.; Yoda, T.; Uchida, T.; Tanamura, Y.; Yamashita, T.; Teramae, N. *Nat. Mater.* **2004**, *3*, 337. (b) Lu, Q.; Gao, F.; Komarneni, S.; Mallouk, T. E. *J. Am. Chem. Soc.* **2004**, *126*, 8650. (c) Platschek, B.; Koehn, R.; Doeblinger, M.; Bein, T. *ChemPhysChem* **2008**, *9*, 2059. (d) Platschek, B.; Koehn, R.; Doeblinger, M.; Bein, T. *Langmuir* **2008**, *24*, 5018.

(18) (a) Fukumoto, H.; Nagano, S.; Kawatsuki, N.; Seki, T. *Chem. Mater.* **2006**, *18*, 1226. (b) Tolbert, S. H.; Richman, E. K. U.S. Pat. Appl. Publ. US 2006278158.

(19) (a) Miyata, H. *Microporous Mesoporous Mater.* **2007**, *101*, 296. (b) Richman, E. K.; Brezesinski, T.; Tolbert, S. H. *Nat. Mater.* **2008**, *7*, 712.

(20) (b) Yamauchi, Y.; Sawada, M.; Komatsu, M.; Sugiyama, A.; Osaka, T.; Hirota, N.; Sakka, Y.; Kuroda, K *Chem. Asian J.* **2007**, *2*, 1505.

(21) Yamauchi, Y.; Sawada, M.; Sugiyama, A.; Osaka, T.; Sakka, Y.; Kuroda, K. *J. Mater. Chem.* **2006**, *16*, 3693.

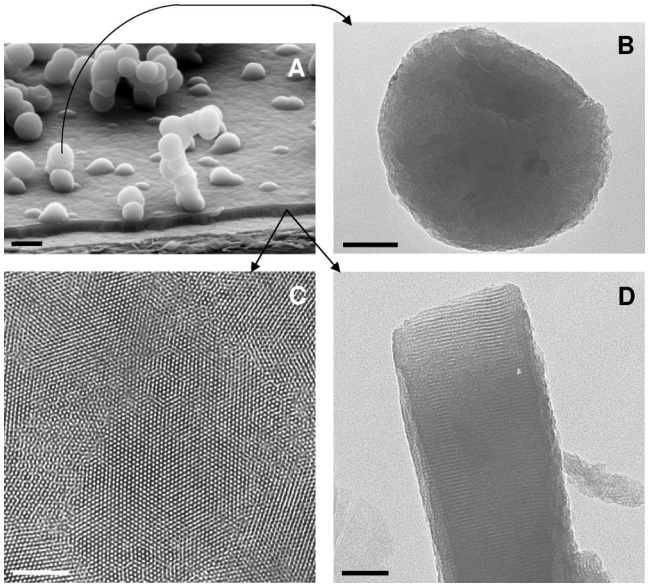

Figure 1. (A) FE-SEM and (B−D) TEM images of an EASA-produced silica film: (B) view of a sphere, (C) top view, and (D) cross-section of the mesoporous silica film. These images correspond to a film deposited on ITO at −1.3 V for 20 s from a sol containing 340 mmol L^{-1} TEOS with $n_{CTAB}/n_{TEOS} = 0.32$. The scale bars represent 50 (A, C, D) or 100 nm (B).

We have recently discovered that electrochemistry is likely to induce self-assembly of cetyltrimethylammonium bromide (CTAB)-templated silica thin films on various conducting supports, with mesopore channels oriented perpendicular to the solid surface over wide areas.[22] The method is very simple and versatile, combining the electrochemically driven self-assembly of surfactants at solid/liquid interfaces[23] and sol−gel electrodeposition.[24] Briefly, it involves the application of a suitable cathodic potential to an electrode immersed in a hydrolyzed sol solution containing a surfactant template (i.e., CTAB) to generate the hydroxide ions that are necessary to catalyze polycondensation of the precursors in the form of a silica thin film made of hexagonally packed one-dimensional channels of about 3 nm in diameter, which are growing normal to the electrode surface. The versatility of the method enables deposition on substrates of different nature, but unfortunately, these films have only been prepared on conductive surfaces so far. Figure 1 shows that the deposit is actually constituted by a continuous thin film of homogeneous thickness (submicrometer) with some overlying aggregates made of individual spheres (see part A). Only the thin film is well-mesostructured and oriented (see parts C and D), whereas the spheres are characterized by ill-defined structure (see part B). Functionalized and oriented mesoporous thin films (i.e., with aminopropyl groups[25]) can be also prepared in one step by this method. However, no attempt was made in these first reports neither to characterize the structure of these films directly on their support (i.e., without removing them as required for TEM observation) nor to investigate all parameters likely to affect this novel so-called electro-assisted self-assembly (EASA) method and the properties of the resulting mesoporous films.

The aim of this paper is to provide a detailed investigation of the EASA process. At first X-ray diffraction techniques, especially at grazing incidence (GIXD), will be applied to characterize the mesoporous silica films without removing them from the support to evaluate their long-range order. Then, the effect of various experimental parameters (mainly the starting sol composition) will be studied with respect to the properties of the final films (degree of organization, pore orientation, thickness, pore size). They include the type and concentration of alkylammonium surfactant, the concentration of the alkoxysilane precursor, and the way of electrodeposition (galvanostatic versus potentiostatic). Special attention was given to prepare aggregate-free films. Because of the importance of permeation through these films for practical applications, electrochemical methods were also applied to characterize their permeability to selected redox probes (mainly ferrocene ethanol, FcEtOH, as it is expected not to interact with the silica matrix).

2. Experimental Section

2.1. Chemical andReagents. Tetraethoxysilane (TEOS, 98%, Alfa Aesar), ethanol (95−96%, Merck), $NaNO_3$ (99%, Fluka), HCl (37%, Riedel de Haen) and dodecyltrimethylammonium bromide (C_{12}TAB, 99%, Fluka), tetradecyltrimethylammonium bromide (C_{14}TAB, 99%, Sigma), cetyltrimethylammonium bromide (CTAB or C_{16}TAB, 99%, Acros), and octadecyltrimethylammonium bromide (C_{18}TAB, 98%, Aldrich) were used as received for films synthesis. Ferrocene ethanol (FcEtOH, Alfa Aesar), potassium hexacyanoferrate(III) ($K_3Fe(CN)_6$, Fluka), and potassium hydrogen phthalate (KHP, Fluka) were analytical grade. All solutions were prepared with high purity water (18 MΩ cm^{-1}) from a Millipore milli-Q water purification system.

2.2. Preparation of Mesoporous Films. Electro-assisted deposition of mesoporous silica thin films was achieved using indium−tin-oxide (ITO) plates (surface resistivity = 8−12 Ω, Delta Technologies) and glassy carbon (Alfa-Aesar) electrodes. A typical sol consisted of 20 mL of ethanol, 20 mL of an aqueous solution of 0.1 M $NaNO_3$ to which were added 50−340 mmol L^{-1} TEOS and 12−544 mmol L^{-1} surfactant under stirring. HCl was added in order to reach a pH close to 3. The surface of the electrode was delimited by a round seal (10 mm inner diameter) on which was placed a Teflon reservoir containing the sol. A cathodic potential (−1.3 V on ITO, −2.2 V on glassy carbon) or a current density (typically −0.74 mA cm^{-2}) was applied for certain duration. The electrode was then quickly removed from the solution and immediately rinsed with distilled water. The deposit was finally dried and aged overnight in an oven at 130 °C. Surfactant extraction was typically carried out by immersing the film in an ethanol solution containing 0.1 mol L^{-1} HCl under moderate stirring for 5 min.

2.3. Instrumentation and Analytical Procedures. The film morphology was characterized by transmission electron microscopy (TEM) using a Philips CM20 microscope at an acceleration voltage of 200 kV. The samples were prepared by mechanically removing some pieces of the films which were then supported on a carbon-coated copper grid. FE-SEM images were obtained using a Stereoscan 440 SEM apparatus (LEICA) having a 4.5 nm resolution.

(22) Walcarius, A.; Sibottier, E.; Etienne, M.; Ghanbaja, J. *Nat. Mater.* **2007**, *6*, 602.
(23) Choi, K.-S.; McFarland, E. W.; Stucky, G. D. *Adv. Mater.* **2003**, *15*, 2018.
(24) (a) Shacham, R.; Avnir, D.; Mandler, D. *Adv. Mater.* **1999**, *11*, 384. (b) Deepa, P. N.; Kanungo, M.; Claycomb, G.; Sherwood, P. M. A.; Collinson, M. M. *Anal. Chem.* **2003**, *75*, 5399. (c) Sayen, S.; Walcarius, A. *Electrochem. Commun.* **2003**, *5*, 341. (d) Sibottier, E.; Sayen, S.; Gaboriaud, F.; Walcarius, A *Langmuir* **2006**, *22*, 8366.
(25) Etienne, M.; Goux, A.; Sibottier, E.; Walcarius, A. *J. Nanosci. Nanotechnol.* **2008**, *8*, in press.

The films crystallinity was characterized by X-ray diffraction (XRD) in Bragg−Brentano geometry using a Panalytical X'Pert Pro diffractometer operating with a copper cathode ($\lambda_{K_{\alpha 1}} = 1.54056$ Å) and by grazing-incidence X-ray diffraction (GIXD) using a Nonius Kappa CCD diffractometer[26] equipped with an ApexII CCD detector (copper cathode ($\lambda_{K_{\bar{\alpha}}} = 1.54184$ Å) (see Figure S1 in the Supporting Information; the usefulness of such a dedicated transmission X-ray diffraction diffractometer for the study of thin films was proved in a previous study[26]). GIXD patterns were recorded by performing Kappa scans at fixed Omega orientation (±90°) with a scan width of 0.4° (exposure time 17×10^3 s/°). The measurements of different areas of the sample were then performed by changing the value of the Phi angle of the goniometer. The large sample-to-detector distance was checked using a sample of known lattice parameter,[27] and the beam size was collimated to a diameter of 350 μm. Uncertainties on the measured lattice parameters were estimated from multiple measurements and were found to be less than 0.2 Å. These two diffraction methods do not need any additional sample preparation, the measurement being performed directly on the substrate.

All electrochemical measurements were carried out at room temperature with an Autolab PGSTAT-12 potentiostat (Eco Chemie) monitored by General Purpose Electrochemical System Software. Experiments were carried out in a three-electrode cell using a stainless steel foil as counter-electrode, a silver wire coated with silver chloride as pseudoreference electrode, and ITO or glassy carbon as working electrodes.

The film permeability was characterized by cyclic voltammetry (qualitative analysis) and hydrodynamic amperometry (quantitative analysis) using $Fe(CN)_6^{3-}$ and FcEtOH as electroactive probes (0.5 mmol L^{-1} in 0.05 mol L^{-1} potassium hydrogen phthalate). Cyclic voltammograms have been recorded at a scan rate of 20 mV s^{-1}. Quantitative analysis of permeability through the mesoporous silica films was performed by hydrodynamic amperometry in the flowing mode[27] using a home-built wall-jet electrochemical setup. It consisted in a syringe needle positioned 10 mm from the analyzed film, perpendicular to the film surface (pointing to the center of the electrode surface area defined by a seal (0.4 mm inner diameter)). A platinum wire and an Ag/AgCl reference (Metrohm) complete the device. Volume flow rates (V) were controlled by a peristaltic pump.

3. Results and Discussion

3.1. Structural Characterization. *3.1.1. Preliminary Observations.* Even if TEM pictures (Figure 1) fully supports the orthogonal orientation of mesopore channels and the high level of mesostructural order, these data have been obtained after removing some parts of the film from its support. Such mechanical removal and transfer onto a TEM grid may lead to some physical damages and portions of the film are expected to curl upon transfer to the grid (like a thin sheet of paper falling down on a nonplanar surface), which might contribute to biased observations by TEM. It is thus important to use a technique likely to characterize the structure of the film directly on its support. X-ray diffraction in the Bragg−Brentano geometry (which would have resulted in well-defined diffraction lines for 2D hexagonal mesostructures oriented parallel to the substrate or in case of 3D hexagonal mesostructures[7a,28]), however, is not suited to evidence mesopore channels wel-aligned along the z axis, as confirmed in Figure 2 (inset of part B) for an aggregate-free mesoporous silica thin film. On the other hand, this XRD technique gave rise to a broad diffraction peak with a maximum intensity at 2.8° (2θ), which can be attributed to the particles and aggregates formed on top of the oriented mesoporous thin film (Figure 2). This is especially visible for the much thicker heterogeneous deposits made of numerous aggregates and the signal remained even noticeable after removing most of the aggregates, which can be easily made with the aid of a simple scotch tape while maintaining intact the thin mesoporous film of interest (compare FE-SEM images E and F in Figure 2). This broad XRD signal is attributed to long-range order (see below) in the templated silica spheres, which was of course more intense (image 2A) in the presence of larger amounts of particulate aggregates (image 2E) and much less (image 2B) when most of them have been removed (image 2F).

More appropriate approaches likely to identify both in-plane and out-of-plane structural organization are the two-dimensional X-ray diffraction or small-angle X-ray scattering using grazing incidence mode (GIXD or GI-SAXS, see for example references[8b,29]). This would allow demonstrating the regular vertical orientation of mesopores, quantifying the periodicity of the mesostructure, and evaluating if preparation conditions could affect this organization. Images 2C and 2D illustrate the two-dimensional diffraction patterns obtained for a thin film prepared by EASA, respectively, before and after removal of most aggregates. Considering first the film with few silica spheres, the GIXD pattern exhibits well-defined diffraction spots in the equatorial plane (image 2D). This proves that mesopore channels are aligned perpendicular to the underlying support. The mesostructure can be indexed to a hexagonal lattice with a parameter of 40.7(±0.2) Å. The simultaneous presence of the (10), (11), (20), and (21) signals indicates that the sample is made of hexagonal domains of regularly packed mesopore channels. Each domain has the same *p6m* symmetry with *C*6 rotation axis perpendicular to the surface (yet with in-plane rotation from one domain to another with clearly visible grain boundaries, see image 1C, as a result from nucleation/growth), showing that the film is highly organized and textured. The average coherence length for each domain is around 200 nm. Similar multiple domains in mesoporous silica films were also observed elsewhere for deposits obtained by evaporation.[30] Additional rings of very low intensities related to the intense in-plane diffraction can be also noticed from the GIXD pattern, which are much more intense in thicker films (image 2C); these signals are explained by the presence of particulate aggregates displaying randomly distributed domains of the same hexagonal structure as the underlying film. Note that the relative position of the beam stop versus the incoming beam direction was slightly offset in these particular experiments to enable

(26) Aubert, E.; Wenger, E.; Link, M.; Assouar, B.; Didierjean, C.; Lecomte, C. *J. Appl. Crystallogr.* **2006**, *39*, 919.
(27) Aubert, E.; Porcher, F.; Souhassou, M.; Petříček, V.; Lecomte, C. *J. Phys. Chem. B* **2002**, *106*, 1110.
(28) Massari, A. M.; Gurney, R. W.; Schwartz, C. P.; Nguyen, S. T.; Hupp, J. T. *Langmuir* **2004**, *20*, 4422.
(29) Jung, J.-I.; Bae, J. Y.; Bae, B.-S. *J. Sol−Gel Sci. Technol.* **2004**, *31*, 179.
(30) Platschek, B.; Petkov, N.; Bein, T. *Angew. Chem., Int. Ed.* **2006**, *45*, 1134.

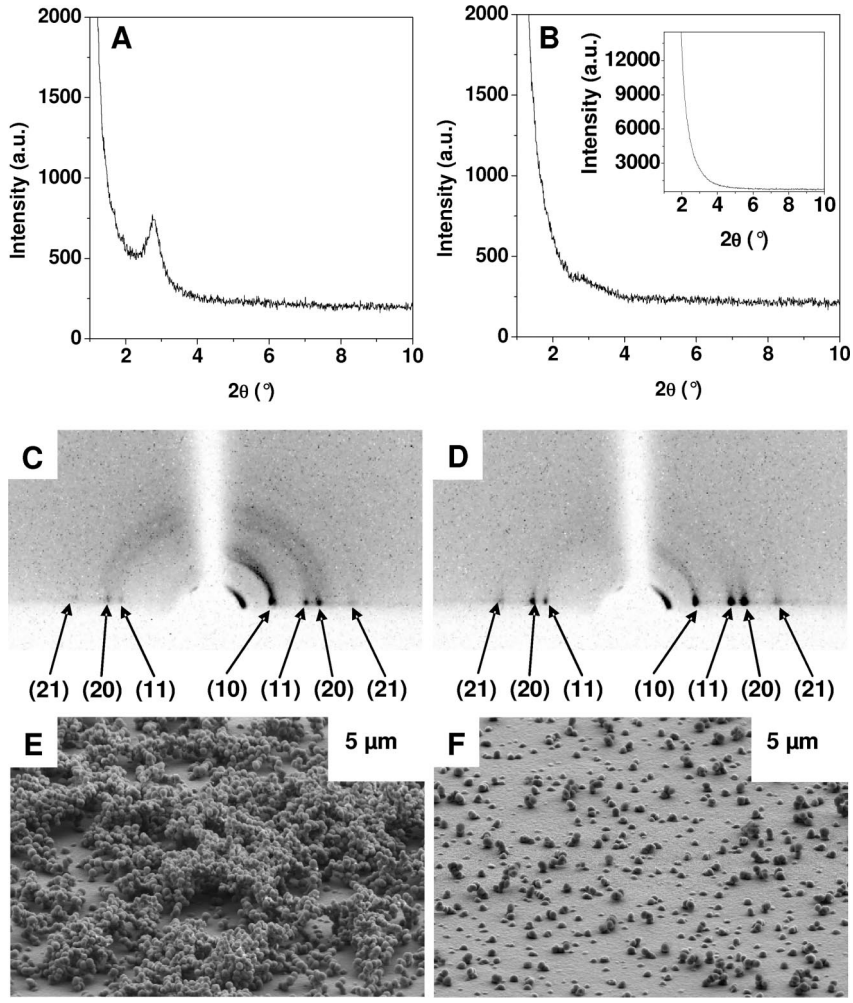

Figure 2. (A, B) Bragg−Brentano XRD patterns (Cu $K\alpha_1$ radiation), (C, D) GIXD patterns and (E, F) FE-SEM images of an EASA-produced silica film: (A, C, E) as-deposited film, (B, D, F) the same film after removal of most particulate aggregates. These data correspond to a film deposited on ITO (20 s electrolysis) except the inset of (B), which represents the XRD pattern obtained for an aggregate-free thin film deposited on gold (5 s electrolysis).

visualization of the (10) spot on one side of the image. Experiments were also performed with a centered beam stop but (10) spots cannot be seen on the resulting patterns due to the beam stop size (see one example in Figure S2 of the Supporting Information).

The surfactant template can be removed from the thin layer by either solvent extraction (ethanol containing 0.1 mol L^{-1} HCl, for 5 min) or calcination (450 °C for 30 min). These two methods have been applied and the resulting films have been characterized by GIXD. The patterns indicate that the high degree of mesostructural order and vertical orientation of mesopore channels are maintained after template removal (independently of the extraction method, see Figures S2 and S3 in the Supporting Information). The well-defined diffraction spots in the equatorial plane confirm that no change in the lattice parameter (41 Å) has been observed, contrary to mesoporous silica thin films having other than vertical porosity structures (cubic, hexagonal 3D, wormlike, hexagonal *p6m*) for which significant lattice contraction has been reported.[28] Another possible explanation is that silica network is formed here in basic medium, whereas acid catalysis is usually used in EISA and the basic catalysis in known to lead to denser network.

3.1.2. Conditions To Get Oriented Mesostructures; Influence of the Sol Composition. The sol composition, especially the CTAB/TEOS molar ratio, is known to dramatically affect the structure (degree of organization and mesostructure type) of mesoporous silica films prepared by EISA.[6,8] GIXD and TEM have been used here to evaluate the influence of the synthesis medium composition on the EASA process and particular attention was paid to define the conditions enabling to get highly structured and oriented mesoporous films. The starting sol giving rise to such well-ordered and oriented mesostructures was composed of a water/ethanol mixture (50:50 volume ratio), 340 mM TEOS, and 109 mM CTAB (i.e., corresponding to a CTAB/TEOS molar ratio of 0.32). TEOS and CTAB concentrations and CTAB/TEOS molar ratios were first varied systematically in order to evaluate their importance on the final film structure. Table 1 gives an overview of the concentration ranges that have been studied and provides information on the structure of deposits.

Contrary to mesoporous silica films prepared by EISA for which the CTAB/TEOS ratio (i.e., in the range 0.1−0.25) is a critical parameter affecting the mesostructure type (hexagonal, cubic or lamellar),[8b] those obtained by EASA were

Table 1. Influence of CTAB and TEOS Concentrations on the Mesostructure Type of Electrogenerated Thin Films; All Other Constituents of the Synthesis Sol Have Been Kept Constant (water/ethanol volume ratio, 50:50; HCl concentration, 1 mM)

	[TEOS] = 50 mM		[TEOS] = 75 mM		[TEOS] = 340 mM		[TEOS] = 650 mM	
CTAB/TEOS molar ratio	[CTAB] (mM)	structure type[a]	[CTAB] (mM)	structure type[a]	[CTAB] (mM)	structure type[a]	[CTAB] (mM)	structure type
0.04					14	A [b]		
0.08					27	HO-A [b,c,s]		
0.16			12	HO [c]	54	HO [c]		
0.32	16	HO [c,s]	24	HO [c]	109	HO [b,c]	208	A [c]
0.64			48	HO [c]	218	HO [b,c]		
1.28			96	HO [c]	435	W [b,c]		
1.60					544	A [b]		

[a] A, non-ordered amorphous; HO, hexagonal packing of oriented mesochannels; W, weakly-ordered films (probably wormlike). [b] TEM observation. [c] GIXD determination. [s] Low signal in GIXD, which probably indicates low level of mesostructuration.

essentially characterized by oriented hexagonal arrays of mesopore channels or poorly organized or nonordered at all. For example, varying the CTAB/TEOS ratio from 0.04 to 1.6 in a sol containing 340 mM TEOS gave rise to highly ordered and oriented hexagonal mesostructures over a rather wide composition range (CTAB/TEOS ratios from 0.16 up to 0.64). Lower CTAB/TEOS ratios led to amorphous (0.04) or poorly ordered (0.08) materials and higher values resulted in a transition to wormlike (1.28) and fully amorphous (1.6) films. A similar trend was observed with using a lower silica concentration (i.e., 75 mM), the optimal range of CTAB/TEOS ratios being, however, slightly shifted to higher values (up to 0.96, see Table 1). Such wide composition range giving rise to highly organized mesoporous silica films by EASA points out the robustness of the process to get hexagonally packed mesopore channels oriented normal to the underlying support. The reason why cubic and hexagonal phases are formed when prepared by EISA while only hexagonal mesostructures oriented perpendicularly to the surface are obtained by EASA has to be found in distinct film formation mechanisms. Although self-assembly polycondensation performed by evaporation occurs first at the film/air interface, the electro-assisted deposition method implies film growing from the electrode surface where surfactant species are organized under potential control in the form of hemimicelles, thereby inducing self-assembly polycondensation in the privileged direction orthogonal to the underlying support upon electrogeneration of the hydroxide catalyst.[22]

For TEOS concentrations studied here (50−340 mM), mesostructuration started to appear at CTAB contents higher than 10−20 mM. Even if it is not straightforward to discuss the concept of critical micellar concentration (CMC) in such complex and evolving medium (ethanol concentration varying with the degree of hydrolysis and condensation, pH higher in the diffusion layer at the electrode/solution interface, potential likely to induce changes in the surfactant organization at the electrode surface[23]), one can notice that oriented mesoporous silica films start to be formed slightly below the CMC as reported to be about 30 mM for CTAB in 50:50 water/ethanol.[31] The mesostructures are then maintained in CTAB concentration ranges of the same order of magnitude around this estimated CMC value or higher. This confirms that the template phase is not preassembled in its final (hexagonal) form in solution and supports the role played by the applied potential to organize this template in the appropriate configuration (at least transiently) to induce TEOS polycondensation and cooperative self-assembly in the form of oriented mesopore channels. Moreover, one knows that CMC is strongly affected by the water/ethanol ratio (i.e., for CTAB, CMC values of about 6 and 100 mM, respectively, for water/ethanol ratios of 75:25 and 25:75[31]). Attempts to get oriented mesostructures in these media failed, leading to nonorganized deposits when the surfactant concentration was below the CMC or poorly organized (but nonoriented normal to the support) materials when above the CMC (see Figure S4 in the Supporting Information).

The above results have pointed out the crucial point of CTAB concentration on the structure of templated silica films prepared by EASA, showing that highly ordered and oriented mesostructures can be obtained by this method over wide surfactant concentration ranges. These ranges were found to be dependent on TEOS concentrations, the key parameter controlling mesostructuration being the CTAB/TEOS ratio. This parameter is not the only one, however, as a very high concentration of TEOS (650 mM), associated with a high concentration of CTAB (208 mM, to reach a CTAB/TEOS ratio of 0.32), led to nonorganized films. The effect of TEOS concentration will be discussed more below when investigating the factors controlling the thickness of mesoporous films.

3.1.3. Tuning Lattice Parameter. It is known from the literature that increasing the chain length of the surfactant template results in mesoporous silica materials with increasing lattice parameter.[32] The influence of this parameter on mesostructuration of silica films obtained by EASA has been studied using a series of alkyltrimethylammonium bromides bearing 12 (C_{12}TAB, dodecyltrimethyl ammonium bromide), 14 (C_{14}TAB, tetradecyltrimethylammonium bromide), 16 (CTAB), and 18 (C_{18}TAB, octadecyltrimethylammonium bromide) C atoms in their alky chain. Well-defined hexagonal mesostructures aligned normal to the support have been obtained with all surfactants except C_{12}TAB. Figure 3A shows that the lattice parameter increases with the chain length of the surfactant from 38 to 46 Å, which can be expected from the increasing size of micelles formed when passing from C_{14}TAB to C_{16}TAB and to C_{18}TAB. These values are comparable to those reported in the literature for

(31) Besson, S.; Ricolleau, C.; Gacoin, T.; Jacquiod, C.; Boilot, J.-P. *Microporous Mesoporous Mater.* **2003**, *60*, 43.

(32) (a) Li, W.; Han, Y. C.; Zhang, J. L.; Wang, L. X.; Song, J. *Colloid J.* **2006**, *68*, 304. (b) Li, W.; Han, Y. C.; Zhang, J. L. *Colloid J.* **2005**, *67*, 159.

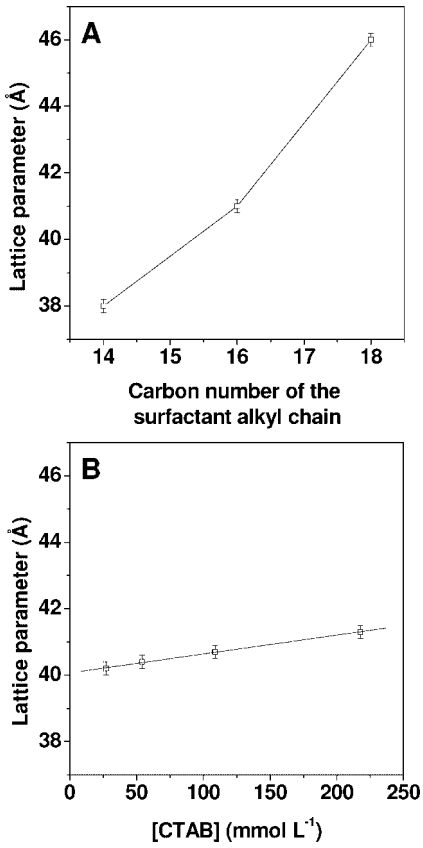

Figure 3. Variation of the lattice parameter determined from GIXD measurements versus (A) the carbon number of the surfactant alkyl chain and (B) the concentration of CTAB in the starting sol. Silica films were electrogenerated on ITO for 20 s (n_{CTAB}/n_{TEOS} = 0.08 to 0.32), 10 s (n_{CTAB}/n_{TEOS} = 0.64), and 5 s (n_{CTAB}/n_{TEOS} = 1.28) from sols containing 340 mmol L^{-1} TEOS.

other mesoporous films prepared by EISA.[32a] Same observation was made independently on TEOS concentration (75−340 mM range) providing the surfactant/TEOS molar ratio was adjusted in the range where mesostructures can be obtained (as defined in section 3.1.2).

On the other hand, varying CTAB concentration in this range ensuring mesostructuration and orientation (i.e., from 27 to 218 mM when using 340 mM TEOS or from 12 to 96 when using 75 mM TEOS) led to measurements of lattice parameters close to 41 Å (as expected for CTAB-templated materials[32a]), but evolving slightly with the surfactant concentration. As shown in Figure 3B, a linear dependence of the lattice parameter versus CTAB concentration was observed, with values extending from 40.2 to 41.3 Å from the lower to the higher CTAB concentration. This behavior could be related to a change in surfactant packing when decreasing the surfactant concentration.

3.2. Optimization of the EASA Process. *3.2.1. Thin Oriented Mesoporous Silica Film versus (Unwanted) Aggregates.* Experimental conditions to get a highly organized and oriented mesoporous silica film have been defined above but no attention was paid to the presence of particulate aggregates and to the way to obtain aggregate-free deposits. One already knows that these two forms (uniform thin film and heterogeneously aggregated particles) result from the particular mechanism of the EASA process, which is characterized by a first slow growing of the oriented mesoporous thin film and then a fast deposition step due to bulk gelification at the electrode/solution interface.[22] Such a two-step process with distinct deposition rates is typical for sol−gel films obtained by electro-assisted deposition, even in the absence of template.[24d] This is due to the fact that the polycondensation catalysts (hydroxide ions) are produced in a region at the electrode/solution interface much thicker (∼100 μm range) than the thickness of the final film (∼100 nm range). With the goal to define the most appropriate conditions leading to the formation of aggregate-free mesoporous thin films, the influence of both TEOS and CTAB concentrations on growing rates has been investigated on the basis of thickness measurements by FE-SEM. Most conclusions can be drawn from results presented in Figure 4, where the effects of surfactant and silica precursor concentrations have been distinguished (see parts A and B for CTAB and C and D for TEOS), and where data obtained for the thin mesoporous films (parts A and C) and the whole deposits (parts B and D) have been presented separately.

Let us first consider the thin mesoporous film of interest. Results in parts A and C of Figure 4 indicate clearly that film thickness was independent of CTAB concentration whereas it increased linearly with TEOS content. Indeed, using 340 mM TEOS and varying CTAB concentration from 54 to 218 mM (i.e., a concentration range where oriented mesostructures can be formed, see Table 1), gave rise to mesoporous films of constant thickness close to 270 nm (30 s deposition time, see curve a in Figure 4A). It is noteworthy that this behavior was restricted to the CTAB concentration domain ensuring oriented mesostructuration (shifts can occur out of this domain as illustrated in Figure 4A for 435 mM CTAB leading to a thickness of 160 nm corresponding to a poorly ordered film). Mesoporous films of constant thickness were also observed when using 75 mmol TEOS (see curve b in Figure 4A) but, in this case, values were lower (i.e., 50−60 nm, for 20 s deposition time). This suggests that TEOS concentration is likely to influence film thickness, which is better shown in part C of Figure 4 from experiments carried out in the same deposition conditions (20 s electrolysis at −1.3 V) and variable TEOS contents. Increasing TEOS contents from 50 to 340 mM, while keeping the same CTAB/TEOS molar ratio (0.32), resulted in a linear relationship between the precursor concentration and the resulting film thickness (Figure 4C). All thin films displayed the oriented hexagonal mesostructure (Table 1). This indicates that kinetic of deposition is faster in the presence of more concentrated TEOS because the presence of more precursors increases the quantity of condensed matter and thus the deposition rate. The thickness of this oriented mesoporous film can be controlled (submicrometer range) over a rather wide TEOS concentration range.

The results obtained from thickness measurements on the whole films (uniformly oriented mesoporous deposit + particulate aggregates) were significantly different (see parts B&D in Figure 4). At low TEOS concentrations, up to 125 mM, few particles were formed in addition to the thin mesoporous film whereas numerous and bigger particulate aggregates were deposited at larger precursor concentrations, giving rise to much thicker heterogeneous materials (e.g., 4

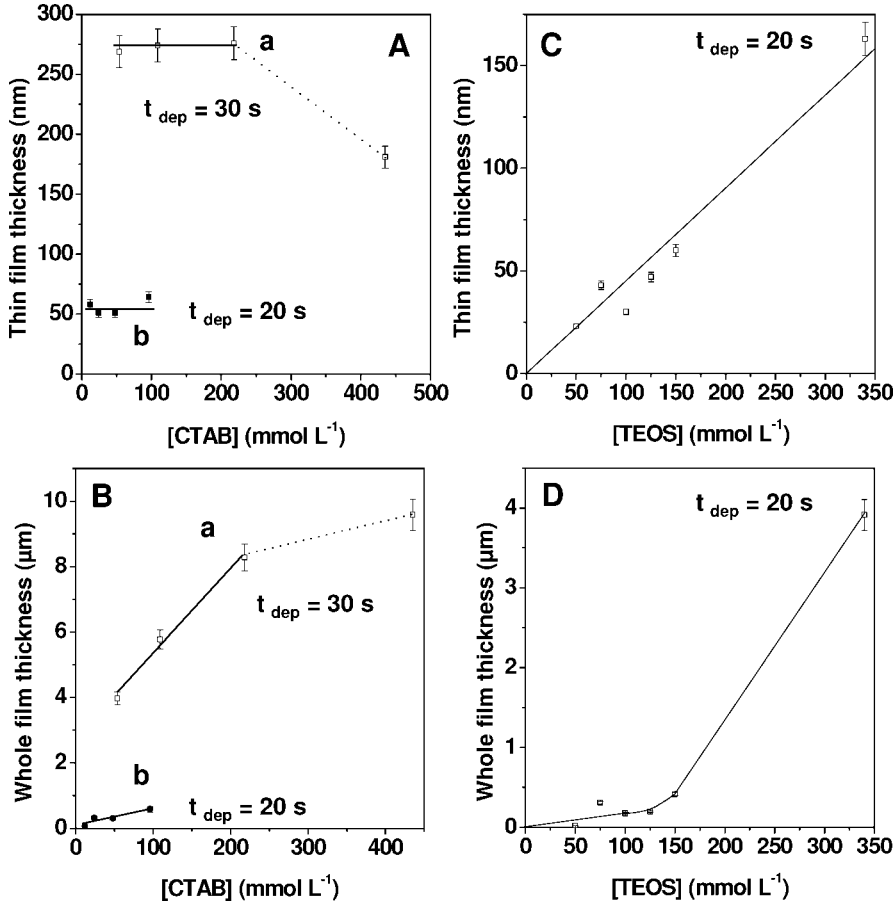

Figure 4. (A, C) Variation of thickness of mesoporous silica thin films as a function of the (A) CTAB and (B) TEOS concentrations. (B, D) Variation of thickness of the whole film (thin mesoporous film and particulate aggregates) as a function of (B) CTAB and (D) TEOS concentrations. (A, B) The films were electrogenerated on ITO plates for 20 s (circle) or 30 s (square) from sols containing 75 mmol L^{-1} (circle) or 340 mmol L^{-1} (square) TEOS and various CTAB concentrations. (C, D) The films were deposited on ITO plates for 20 s from sols containing various concentrations in TEOS with constant $n_{CTAB}/n_{TEOS} = 0.32$.

μm thick deposit with 340 mM of TEOS). The amount of aggregates was also very sensitive to CTAB concentration. As illustrated in Figure 4B, thickness of the whole deposit was found to increase regularly with CTAB concentration and growing was even faster when using more concentrated TEOS (i.e., compare curves a and b, respectively, for 340 mM and 75 mM TEOS). It seems thus that high CTAB and high TEOS concentrations accelerate gelification processes occurring at the electrode/solution interface (i.e., in the diffusion layer), generating the deposition of a much higher amount of particulate aggregates.

Taking in mind the above data and the previously reported influence of electrodeposition time (uniform thin films at short times and heterogeneous thick deposits at longer times[22]), one can now define the most appropriate conditions to get aggregate-free mesoporous thin films. They include short or moderate deposition times (typically 10−20 s at −1.3 V on ITO or 5−10 s at −1.2 V on gold), a TEOS concentration lower than 125 mM and a low CTAB/TEOS ratio (no more than 0.32). An example of such a film is illustrated in Figure 5, showing that highly ordered and oriented mesopore channels are obtained in a thin film of uniform thickness (about 40 nm in this case), without aggregates (only very few silica spheres randomly distributed over the thin film). High level of mesostructural order and vertical orientation of mesopores are also confirmed by the

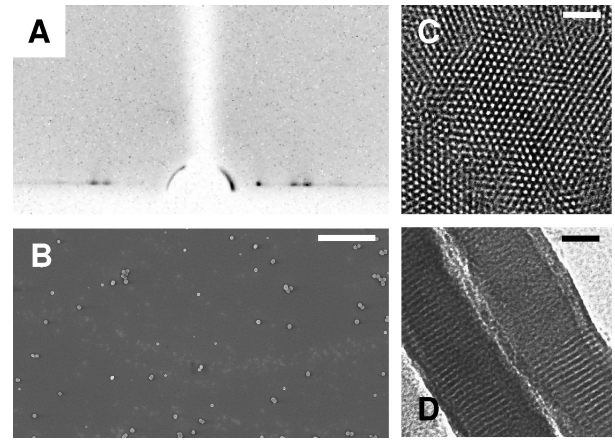

Figure 5. (A) GIXD pattern, (B) FE-SEM top view, and (C, D) TEM top and cross-section views of an electrodeposited mesoporous silica film obtained from a sol containing 75 mmol L^{-1} TEOS with $n_{CTAB}/n_{TEOS} = 0.32$ (deposition duration = 20 s). The scale bars represent (B) 5 μm and (C, D) 20 nm.

GIXD pattern via the only presence of diffraction spots in the equatorial plane and absence of any out-of-plane ring. In such a way, aggregate-free films can be obtained with thicknesses that can be tuned in the 20−50 nm range. It is not obvious to increase the thickness of this oriented film by multilayer formation (i.e., by performing several depositions in the optimal conditions) as the polycondensation

catalyst is produced in a thick diffusion layer (~100 μm), which results in unwanted memory effects leading to aggregates formation between each successive electrogenerations.

3.2.2. Electro-Assisted Deposition in the Galvanostatic Mode. Until now, all films generated by EASA[22,25] have been obtained under potentiostatic conditions (i.e., by applying a suitable cathodic potential to the electrode to generate the hydroxide catalysts of polycondensation). A complete description of the effect of applied potential and electrolysis duration has been given previously.[22] This approach requires the application of a potential value that can be markedly different when passing from a substrate to another one (e.g., optimal potential was typically −1.3 V on ITO and −2.2 V on glassy carbon) due to variable overpotentials depending on the nature or surface state of the electrode material (as classically observed in electrochemistry[33]). To overcome the need of optimizing the applied potential each time a novel electrode substrate is used, an alternative route to generate the hydroxide ions is the application of a current density instead of a potential. This galvanostatic mode provides the advantage to enable fine-tuning of film growth and thickness control whatever the nature and the surface area of the underlying electrode. In doing such, the electrode potential is automatically adjusted by the galvanostat upon application of the desired electrolysis current. For example, applying a current density of −0.74 mA cm^{-2} to glassy carbon (GC) and ITO plates, for the same deposition time (20 s), resulted in distinct potential values depending on the substrate (i.e., about −2.2 V on GC and −1.4 V on ITO). The resulting film thicknesses were almost similar in both cases, 265 nm on GC and 270 nm on ITO (see Figure S5 in the Supporting Information). TEM and GIXD measurements confirm that such deposition mode does not affect the final mesostructure (same lattice parameter, orthogonal orientation of mesochannels, highly ordered hexagonal packing of mesopores).

Even more interesting is the possibility offered by the galvanostatic mode to adjust accurately the deposition conditions by simple variation of the current density and electrolysis duration independently on the nature of the electrode. Figure 6 shows the variation in thickness for mesoporous films deposited on ITO applying various current densities for increasing periods of time. Whatever the current density, the film thickness was always found to grow linearly with the deposition time, here between 5 and 20 s. Moreover a direct correlation can be drawn between current density and film thickness for the same given deposition time (see inset in Figure 6 for 8 s electrolysis). The growth rate was about 14, 19, and 34 nm s^{-1} when applying −0.74, −1.5, and −3 mA cm^{-2}, respectively. These rates are constant independently on the nature of the electrode whereas film deposition by potential control were characterized by growth rates strongly dependent on the applied potential and these variations were different from one electrode substrate to another one.[22] Finally, all conclusions established above

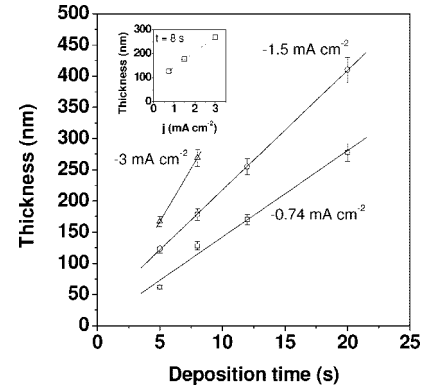

Figure 6. Variation in thickness of thin films deposited galvanostatically on ITO at various currents densities: −0.74 (□), −1.5 (○), and −3 mA cm^{-2} (△), as a function of the deposition time. Inset: Variation in thickness of thin films deposited for 8 s, as a function of the current density.

remain valid, especially the fact that aggregates-free thin films can be obtained by applying "soft" deposition conditions (diluted precursor solution, short deposition times and slow generation of the catalysts, this latter being achieved here by applying a small current density).

3.3. Electrochemical Characterization of Mass Transport Issues. Oriented mesoporous silica thin films are attractive from many points of view, but a straightforward application of such materials deposited onto electrode surfaces concerns the field of electrochemistry.[2d,5e,34] The rate-determining step in electrochemical measurements is governed by the speed of both electron transfer and mass transport of redox probes to the electrode surface. For a selected redox probe and a given electrode material, the speed of electron transfer is defined and constant if no change is made to the electrode/solution interface. In the presence of a film deposited onto the electrode surface, additional resistance to mass transport can occur as such film can act as a physical barrier slowing down the diffusion of redox probes from the solution to the electrode surface. This is indeed the case of mesoporous silica films on electrodes for which electrochemical responses were found to be dependent on structure type and porosity.[34] We have thus evaluated here if the experimental conditions applied to prepare oriented mesoporous films by EASA are likely to affect, or not, the electrochemical behavior of the resulting modified electrodes.

Mass transport issues at film-modified electrodes can be characterized by electrochemical techniques, either qualitatively by cyclic voltammetry (CV) or quantitatively by hydrodynamic voltammetry (using rotating disk electrodes[33] or in flowing conditions using a wall-jet configuration[27]) or electrochemical impedance spectroscopy.[35] Basic CV characterization has been reported previously for films prepared on gold or glassy carbon electrodes[22] and is reminded here for films prepared on ITO (see Figure S6 in the Supporting Information). Similar conclusions can be drawn. First, before template extraction, the films are totally impermeable to $Fe(CN)_6^{3-}$ and $Ru(bpy)_3^{2+}$ redox probes, confirming that

(33) (a) Park, S. S.; Ha, C. S. *Chem. Mater.* **2005**, *17*, 3519. (b) Park, S. S.; Ha, C. S. *Chem. Rec.* **2006**, *6*, 32. (c) Ogawa, M.; Kikuchi, T. *Adv. Mater.* **1998**, *10*, 1077. (d) Gosh, K.; Vyas, S. M.; Lehmler, H. J.; Rankin, S. E.; Knutson, B. L. *J. Phys. Chem. B* **2007**, *111*, 363.

(34) Bard, A. J.; Faulkner, L. R. *Electrochemical Methods: Fundamentals and Applications*, 2nd ed.; John Wiley and Sons: New York, 2000.

(35) Etienne, M.; Quach, A.; Grosso, D.; Nicole, L.; Sanchez, C.; Walcarius, A. *Chem. Mater.* **2007**, *19*, 844.

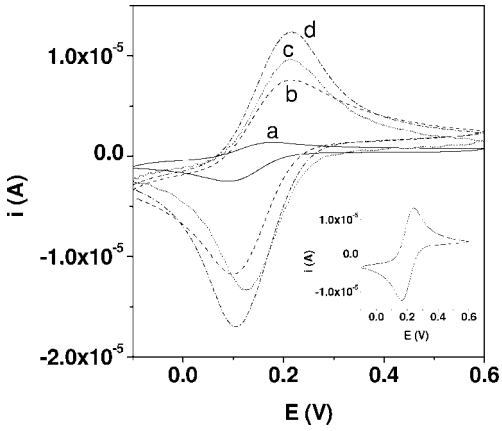

Figure 7. Cyclic voltammograms recorded in 0.05 M hydrogen phthalate solutions containing 0.5 mmol L^{-1} FcEtOH at ITO electrodes covered by mesoporous silica thin films deposited at −1.3 V with various surfactants: (a) C_{12}TAB, (b) C_{14}TAB, (c) C_{16}TAB, and (d) C_{18}TAB. All curves have been obtained after surfactant extraction. The response of the bare electrode is given in inset. The surfactant/TEOS molar ratio was adjusted depending on the surfactant. It was 0.5 for C_{12}TAB and C_{14}TAB, and 0.32 for C_{16}TAB and C_{18}TAB.

mesoporous silica was homogeneously deposited in the form of a crack-free film over the entire electrode surface, whereas a small response was observed for ferrocene ethanol (FcEtOH) because of its solubilization into the liquid crystalline phase formed by the surfactant in mesopore channels (leading to an anodic shift in peak potentials relative to solution-phase FcEtOH.[36] After template removal, the film became porous to all solution-phase redox probes but some repulsion to $Fe(CN)_6^{3-}$ anions and accumulation of $Ru(bpy)_3^{2+}$ cations were observed as a result of the negatively charged silica surface, so that the use of the neutral FcEtOH probe was preferred to characterize diffusion processes without additional electrostatic effects.

Figure 7 shows CV curves recorded using FcEtOH as solution-phase redox probe and bare ITO electrode (inset) or ITO electrodes covered with thin films prepared using C_{12}TAB (curve a), C_{14}TAB (curve b), CTAB (curve c), and C_{18}TAB (curve d). Mesoporous films have been prepared in same conditions and all voltammograms have been recorded after surfactant extraction. As shown, peak currents were found to decrease in intensity when passing from films prepared with C_{18}TAB to C_{12}TAB. This can be attributed qualitatively to slower mass transport through films of smaller porosity. Even more impressive is the very low signal observed for the C_{12}TAB-based film, which was not mesostructurally ordered, pointing out the great interest of oriented mesostructures to enhance mass transfer rates at silica-modified electrodes.

Quantitative characterization of these processes can be made under hydrodynamic conditions, which have been made here via a controlled convection method called wall-jet electrochemistry.[27] In such wall-jet setup, convection is controlled by a solution flow, V (cm^3 s^{-1}), passing through a small capillary positioned at a close distance normal to the electrode surface.[27,34] The plot of $1/I$ (I = current arising from imposing a suitable potential depending on the redox probe, i.e., +0.4 V) versus $1/V^{3/4}$ allows extracting a limiting current (I_{lim}), the value of which depends on the electrochemical process occurring through the thin layer (both electron and mass transfers). Two models have been proposed to describe the electrochemical response of electrodes covered with a thin film whether redox species have access to the electrode surface through pinholes or through a homogeneous membrane.[33] The pinhole model considers small holes regularly distributed through an impermeable layer, whereas the membrane model involves restricted diffusion through a homogeneous film.[33] According to the high density of closely packed mesopore channels characteristics of films prepared by EASA and because no detectable pin-holes were found in the films (as notably confirmed by flat CV responses before surfactant extraction, see curves b in parts A and B in Figure S6 in the Supporting Information), the membrane model has been chosen as the most appropriate hypothesis. In this case, the following equation applies to calculate the rate of the electrochemical process (k_{eff}), which constitutes a direct measurement of permeation (PD_f) through the film for a diffusion-limited process[33]

$$k_{eff} = I_{lim}/(nFAC) = PD_f/d \quad (1)$$

where k_{eff} is the effective rate constant of the electrochemical process, P the partition coefficient between the solution and the film, D_f the apparent diffusion coefficient through the film (cm^2 s^{-1}), d the thickness of the layer (cm), n the number of electron involved in the electrochemical process, F the Faraday constant (C mol^{-1}), A the electrode surface area (cm^2, considered here as the geometric one), and C the concentration of the redox probe in the bulk solution (mol cm^{-3}).

The relevance of this model can be validated with using films prepared in similar conditions but displaying various thicknesses for which a constant permeability is expected. Results of Figure 8A confirm indeed that a linear variation in k_{eff} values versus $1/d$ has been obtained for FcEtOH oxidation at electrodes covered with films of increasing thickness prepared galvanostatically from a sol containing 340 mmol TEOS and 109 mmol CTAB by tuning time and/or current of electrodeposition. For these films, a constant average value of permeability was calculated as $PD_f = 9 \times 10^{-8}$ cm^2 s^{-1}. Assuming absence of (or very weak) interactions between FcEtOH and the film ($P = 1$), this value would correspond to an apparent diffusion coefficient equal to 9×10^{-8} cm^2 s^{-1}, which is a rather high value for mass transfer in such confined environment. Smaller values have been obtained for non templated silica films ($<1 \times 10^{-9}$ cm^2 s^{-1}) or non oriented 3D-hexagonal mesostructures prepared by EISA ($\sim 1 \times 10^{-8}$ cm^2 s^{-1}).[34]

Orthogonal orientation is thus advantageous to impart fast mass transfer of solutes from the external solution to the underlying support, but results of Figure 8B indicate that this might be not so simple with respect to electrochemical applications of mesoporous silica film electrodes. This figure reports the variation of k_{eff} values as a function of CTAB concentration used to generate the mesoporous silica films while keeping constant TEOS concentration (340 mmol L^{-1}) and applying the same deposition conditions for all films.

(36) Wei, T. C.; Hillhouse, H. W. *Langmuir* **2007**, *23*, 5689.
(37) Etienne, M.; Cortot, J.; Walcarius, A. *Electroanalysis* **2007**, *19*, 129.

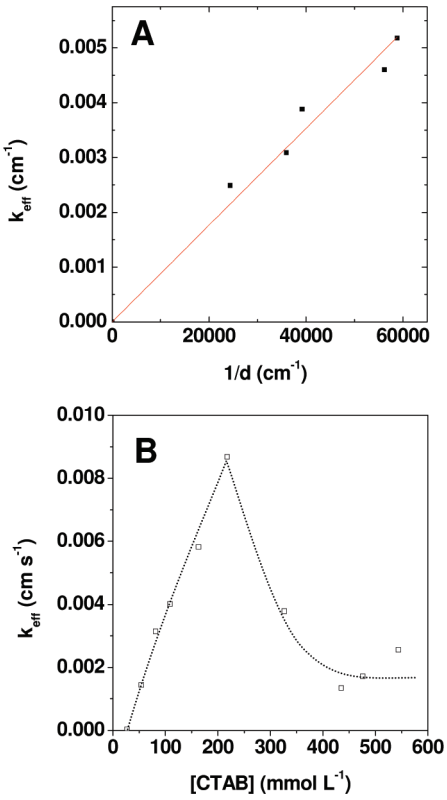

Figure 8. Evolution of the effective kinetic constant, k_{eff}, for FcEtOH oxidation as a function of (A) the inverse of the film thickness, 1/*d*, and (B) the surfactant concentration ([CTAB]). (A) Films have been obtained by galvanostatic deposition for increasing periods of time on ITO from a sol containing 340 mmol TEOS and 109 mM CTAB. (B) Films were electrogenerated on ITO plates for 30 s from sols containing TEOS 340 mmol L^{-1} and increasing CTAB concentrations.

The second part of the curve (i.e., CTAB concentration >218 mM) can be easily explained: one observes a decrease in k_{eff} values from the highest one (9×10^{-3} cm s^{-1} at 218 mM CTAB) down to about 2×10^{-3} cm s^{-1} when increasing CTAB concentration, which is clearly due to restricted mass transport in films becoming progressively less mesostructured or not ordered at all when increasing CTAB concentration in the synthesis medium (Table 1). The first part of the curve is much more surprising, as it corresponds to films prepared in a CTAB concentration range (27−218 nM) where the same oriented mesostructures are obtained (Table 1) with the same thickness (Figure 4A) and almost the same lattice parameter (Figure 3B). In such a case, one would have expected to observe the same permeability properties but Figure 8B shows that effective kinetic constant values were found to decrease significantly when decreasing CTAB concentration used in the synthesis medium. This decrease cannot be reasonably due to restricted diffusion inside mesopore channels (as they are characterized by similar length, orientation and size). A possible explanation would be an additional limitation at the interface between the electrode and the film (making the real surface accessible for the electrochemical reaction lower than the geometric one) or between the film and the solution, which could be due to the presence of bottle necks at the outermost surfaces of the film. This hypothesis is supported by the slow decrease in lattice parameter when decreasing CTAB concentration mostly due to lower packing of surfactant species, which might be especially restrictive at mesopore entrance, inducing additional resistance to mass and/or charge transfer processes. Anyway, even if the reason for such a limitation is not well-understood at this stage, the above results indicate that getting vertically aligned mesopore channels is a prerequisite to ensure fast mass transport through the film, special attention has to be paid to defining the most appropriate synthesis conditions giving rise to highest values of effective kinetic constants, at least if electrochemical applications are concerned.

Conclusions

In this work, we have shown that laboratory GIXD can be applied as a useful technique complementary to TEM to characterize highly ordered and vertically aligned mesoporous silica films prepared onto electrode surfaces by EASA without the need to remove the material from its support. GIXD confirms the dense hexagonal packing of mesopore channels with a lattice parameter equal to 4.1 nm (CTAB-based films), this latter being tunable in the 3.8−4.6 nm range by changing the chain length of the alkyl group of the surfactant. Mesostructured films can be obtained by EASA over a rather wide composition range of the starting sol (i.e., 10−200 mM CTAB and 50−350 mM TEOS) and the final materials were always characterized by the same 2D-hexagonal mesostructure with channels oriented exclusively normal to the underlying support. Film thickness was found to be independent of the CTAB template concentration whereas it was found to grow linearly with TEOS content in the starting sol. This was exploited to prepare aggregates-free thin films that are best obtained in diluted media (i.e., [TEOS] < 125 mM; CTAB/TEOS ratio <0.32) and short deposition time (~10 s). Electro-assisted deposition in the galvanostatic mode enables to avoid overpotential problems associated to potentiostatic conditions. Because of the favorable mesopore orientation, these films are highly permeable to solution-phase redox probes that are likely to reach easily the electrode surface, because of fast mass transfer processes, even if the experimental conditions applied to film formation (notably CTAB concentration) have to be carefully controlled to avoid any additional interfacial limitation.

Acknowledgment. This work was supported by the French National Research Agency (project No. NT05-3 41602 'mesoporelect') and by Institut Jean Barriol (project 'PRIME'). We are also grateful to S. Borensztajn for FE-SEM experiments and to E. Wenger for his help with GIXD measurements. We thank Prof. E. Espinosa for fruitful discussions, and the Service Commun de Diffraction X, Institut Jean Barriol, Nancy-Université, for providing access to crystallographic facilities.

Supporting Information Available: Additional figures (PDF). This material is available free of charge via the Internet at http://pubs.acs.org.

CM8029664